Fiber-Optic Surface Plasmon Resonance Sensors in the Near-Infrared Spectral Region

JEAN-FRANCOIS MASSON, YOON-CHANG KIM, LOUIS A. OBANDO, WEI PENG, and KARL S. BOOKSH*

Department of Chemistry and Biochemistry, Arizona State University, Tempe, Arizona 85287-1604

The sensitivity of fiber-optic surface plasmon resonance (SPR) sensors was improved by a factor of at least thirteen for aqueous solutions by modifying the tip geometry to allow interrogation of the surface plasmon (SP) band in the near-infrared (NIR) region. This was achieved by tuning the angle at the distal end of the SPR sensor to a dual taper of 71° and 19°. Using a low numerical aperture (NA) fiber-optic sensor, NA = 0.12, is necessary to obtain a functional SPR sensor working in the NIR region. Theoretical simulations using the Maxwell equations demonstrated that even higher enhancement is theoretically possible while maintaining a narrow spectral feature upon the excitation of the SP bands on gold surfaces. The manufacture of the SPR sensors yields good agreement between theoretical simulations and experimental observations. To investigate the properties of these fiber-optic SPR-NIR sensors, sucrose solutions ranging from 0 to 15×10^{-3} in mole fraction were utilized. The increased sensitivity of the fiber-optic SPR sensors, when used to monitor biomarkers, would yield lower detection limits. The smaller sensing area, compared to planar or other fiber-optic SPR sensors, combined with an improvement of the sensitivity, would yield a dramatic reduction of the absolute amount detected by biosensors.

Index Headings: **Miniature sensor; Fiber-optic sensors; Surface plasmon resonance; SPR; Refractive index; Biosensors.**

INTRODUCTION

There is a great need for detection of low concentrations or a low number of molecules, especially in the biomedical field. Smaller and highly sensitive sensors are required to achieve low detection limits in both concentration and absolute number of molecules detected. Recently, the use of surface plasmon resonance (SPR) based on fiber optics was reported to achieve low detection limits of biologically relevant molecules.[1–3] One of the main advantages of SPR relies on the possibility of miniaturization without loss of sensitivity. Thus, performing SPR with fiber-optic sensors enables miniaturization by using smaller fibers with the same analytical performance while using smaller sample volumes and detecting a smaller absolute number of molecules. Presented here is a fiber-optic based SPR sensor with a modified tip geometry onto which the sensing area is located, thus enabling smaller sensing areas and excitation of the surface plasmon band in the near-infrared (NIR) region.

Received 16 June 2006; accepted 14 August 2006.
* Author to whom correspondence should be sent. E-mail: booksh@asu.edu

Surface plasmon resonance theory has been extensively described.[4,5] Light undergoing total internal reflection exhibits an evanescent wave. This evanescent wave can excite a standing charge on a thin gold film (Fig. 1). The gold film is typically 50 nm thick. In order for the excitation of a standing charge density wave on the gold film to occur, it must be in contact with a sample of lower refractive index (RI) than the waveguide. Energy transfer occurs when the wave vector of the standing charge k_{sp} and the wave vector of the evanescent wave k_x are equal based on the equations

$$k_{sp} = k_0 \sqrt{\frac{\varepsilon_m \varepsilon_S}{\varepsilon_m + \varepsilon_S}} \tag{1a}$$

$$k_x = k_0 \eta_D \sin\Theta_{inc} \tag{1b}$$

where k_0 is the wave vector of the incident light, ε_m and ε_S are the complex dielectric constants of the metal and the sample respectively, η_D is the refractive index of the waveguide, and Θ_{inc} is the incident angle of the light. From calculations with the Fresnel equations, multiple combinations of incident light angles and wavelengths can excite the standing charge density wave.[5] When k_{sp} in Eq. 1a equals k_x in Eq. 1b the photon is absorbed, shown by a minimum in the reflection spectra (Fig. 1). Figure 1 shows an experimental spectrum of ethanol referenced to a blank air spectrum. The position of the minimum (λ_{SPR}) is indicative of the dielectric constant, or the refractive index, within 100–200 nm of the gold film.

The sensitivity of SPR is influenced by two major factors. First, SPR is most sensitive for processes occurring at the surface. The sensitivity decreases exponentially for processes occurring further from the surface. Second, the sensitivity is also dependent on the wavelength–angle combination used to excite the SP band. Here the case of constant-angle SPR (fiber-optic SPR) will be explained. Solving Maxwell's equations for a gold-coated silica waveguide shows that the sensitivity increases when working at longer wavelengths. Thus, greater sensitivity for SPR is obtained in the NIR spectral region than in the visible region. Typically, fiber-optic SPR is performed in the visible region for aqueous solutions around 600 nm. This is obtained by wave-guiding light in the fiber optics and exciting the SP of a thin gold film on the side of the fiber optics.[6,7] The propagation angle in the fiber-optic sensor is therefore

0003-7028/06/6011-1241$2.00/0

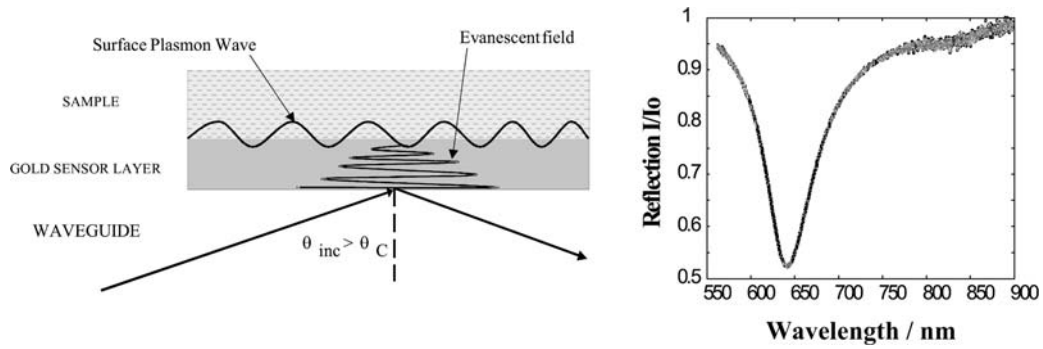

FIG. 1. (**Left**) SPR theory; light excitation of a standing charge on a thin metal film. (**Right**) SPR signal at constant angle.

approximately 80° (Fig. 2). However, the sensitivity is much smaller than performing SPR in the NIR spectral region. There is no report to date of fiber-optic NIR SPR.

Constant-wavelength SPR (Kretschmann configuration) has previously been performed in the NIR region.[8–10] SPR in the NIR region also enables the analysis of thin adsorbed films on the gold surface.[11–14] Spectral fingerprinting of the adsorbate layer was previously observed in the NIR region by SPR.[14] Localized SPR onto silver nanoparticles is also performed in the NIR region by tuning the size of the nanoparticles to exploit the large sensitivity.[15] SPR imaging is also performed in the NIR region.[16,17] Although most variation of SPR exploits the NIR region for the various spectral information gained and the largest sensitivity, fiber-optic SPR has not been performed successfully in the NIR region.

In order to excite the SP band of gold, the propagation angle must be approximately 70° (Fig. 2). This is not accessible using the typical straight sensor SPR sensor configuration. A method to modify the tip geometry of the SPR sensor was introduced by Obando and Booksh with tip angles of 80° and 75° to analyze samples in the visible region around 700 nm.[18] The SPR spectrum was broad with tip modification of 75° or lower angle caused by using fiber with a fairly large NA. The angle distribution was large in the fiber, broadening the SPR dip. A recent development by Kim et al. to utilize low NA fiber for detection of gases by SPR (RI ~ 1.01, Θ_{SPR} ~ 50°) showed promising spectral quality.[19] This technique was applied to perform SPR in the NIR region, enhancing the sensitivity of the SPR measurement using a smaller sensing area.

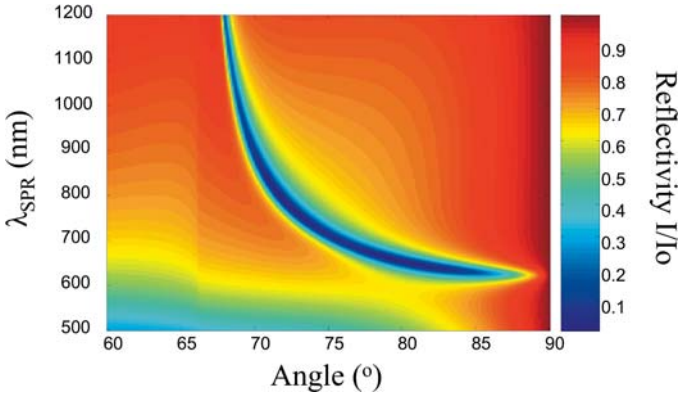

FIG. 2. Theoretical calculation for an aqueous solution (RI = 1.333 RIU) on a 50 nm gold film using silica (RI = 1.457 RIU). The dark blue region corresponds to the position of the matching conditions.

EXPERIMENTAL METHODS

Straight Sensor Surface Plasmon Resonance Sensor. The manufacture of the SPR sensors used in this study has been described previously.[2,18] Here, 400 μm diameter multimode optical fiber with an NA of 0.37 are employed for the sensor tip. However, multimode fibers as narrow as 50 μm could be used. In the current configuration, fibers 45 mm in length are cleaved. An 11 mm long piece of the buffer protecting the fiber is removed and 5 mm is replaced to protect the mirror on the distal end (Fig. 3). The distal end is polished with 5 μm, 1 μm, and 0.3 μm lapping films. The distal end is then washed with isopropanol and the sensor is dried at 100 °C for 10 minutes. A 5 nm adhesion layer of Cr is sputtered on the distal end of the sensor and a 50 nm layer of Au is deposited to form a mirror. The mirror is sealed using oven-cured epoxy, and 10–15 mm of the buffer on the other end of the fiber is removed. The fiber is installed on the connector and fixed in place using oven-cured epoxy. The connector end is polished using 9 μm, 5 μm, and 1 μm lapping films. The cladding on the sensing area is removed using acetone. The sensor is visually inspected using a microscope objective to insure that all the cladding has been removed. Five nanometers (5 nm) of Cr and 50 nm of Au are deposited on the sensing area. The sensor is rotated while being sputtered to ensure an even layer of Cr and Au. The sensor performance is tested in ethanol.

Dual-Taper Surface Plasmon Resonance Sensors. In this study, 486 μm diameter multimode optical fiber with an NA of 0.12 (CeramOptec Industries) are employed for the sensor tip. In the current configuration, fibers 45 mm in length are cleaved. Custom-designed right-triangle polishing chucks were manufactured at 70°/20°, 71°/19°, 72°/18°, and 73°/17° with accuracy on the angle of better than 0.1°. The fiber is mounted on the chuck and the steeper angle is polished first to form the sensing area. The fiber is polished using 6 μm, 1 μm, and 0.3 μm diamond lapping films. The fiber is rotated 180°, mounted on the shallower angle of the chuck to form the mirror, and polished as described previously for the steeper angle. The fiber is installed on the connector and fixed in place using oven-cured epoxy. The connector end is polished using 9 μm, 5 μm, and 1 μm lapping films. The sensing area and the mirror are then carefully washed with isopropanol to remove any impurities on the surface and the sensor is dried at 100 °C for 10 minutes. The sensor is visually inspected using a microscope objective to ensure that the sensing area is clean. A 1 nm adhesion layer of Cr is sputtered on the distal end of the sensor and a 50 nm layer of Au is deposited to form a mirror and the sensing area. The sensor performance is tested in water.

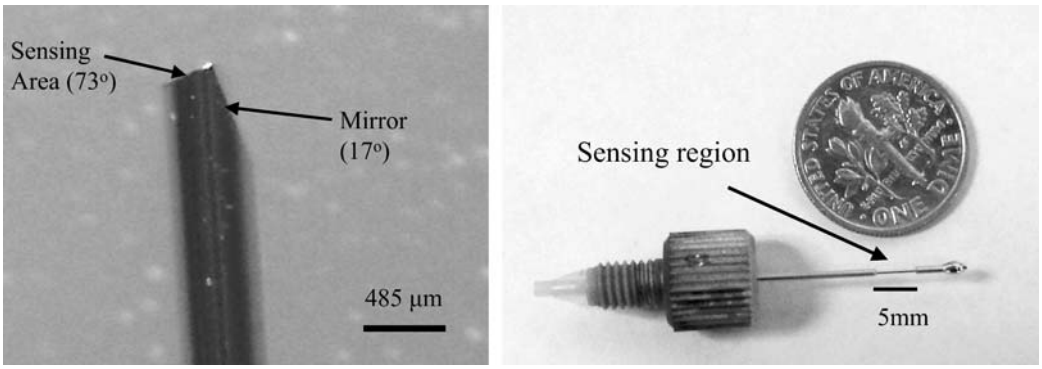

FIG. 3. (**Left**) A photograph under 60× magnification of a dual-tapered fiber-optic SPR sensor. (**Right**) A straight sensor SPR sensor.

Solution Preparation. The sucrose solutions were prepared by weight with measurement accuracy to the nearest 0.1 mg. The eight sucrose solutions ranged in weight fractions from 0 to 15×10^{-3}. All solutions were used within 24 hours of preparation. The solutions' temperature was controlled to 1 °C using a room-temperature water bath.

Refractive Index Measurement. The refractive index of the sucrose solutions was measured using an Abbe refractometer (DR5000, Kruss, Germany) accurate to 1×10^{-5} refractive index units (RIU). The temperature of the refractometer is controlled using a recirculating temperature-controlled water bath. The accuracy of the temperature control of the refractometer is ±0.1 °C.

Surface Plasmon Resonance Measurement. The SPR sensor was exposed for about 5 minutes to the solution in a room-temperature water bath. The solution was stirred during the 5 minutes of exposure. The exposure allows thermal equilibration of the sample. Then, 50 spectra of 200 ms exposure each were acquired and averaged. The spectra are then ratioed to an isopropanol spectrum to remove the lamp profile and obtain the SPR spectrum. The SPR system is composed of a Kaiser spectrometer onto which a Princeton charge-coupled device (CCD) camera is mounted. The resolution of the system is 0.37 nm/pixel covering the range between 530 nm and 910 nm.

RESULTS AND DISCUSSION

Sensor Fabrication. To perform SPR in the NIR region, the incident angle of the light must be tuned to approximately 70°. While it is relatively easy when using the Kretschmann configuration and an imaging configuration to set the incident angle to 70°, it is significantly more complicated with a fiber optics. When using silica fiber optics with a 400 μm diameter and an NA of 0.37, the normal mode of propagation does not include 70°. To excite the SP band at this angle in a fiber-optic sensor, the approach taken here is to modify the shape of the distal end of the fiber. To excite at the distal end of the fiber, the light entering the fiber optics must be collimated. To achieve near collimation, low NA fibers must be used. In this study, SPR is performed on a silica fiber with a 486 μm diameter and an NA of 0.12. The 0.12 NA allows close to collimation into the fiber; although using lower NA fiber would improve the collimation into the fiber, such lower numerical aperture fibers made of silica are not commercially available. A previous article by Kim et al. reported that using a collimating lens did not improve the quality of the spectra.[19] The tip must be a dual-taper geometry, with one side being the sensing area while the second taper acts as a mirror. The dual tapers must be at complementary angles so that the light reflected from the tip is also collimated for maximum collection efficiency.

To modify the tip at the distal end, right-triangle chucks were machined out of stainless steel at complementary angles of 70°/20°, 71°/19°, 72°/18°, and 73°/17°. These chucks were machined with an accuracy of greater than 0.1°. The fiber is mounted on the chuck at the steeper angle first and polished using diamond lapping films until the fiber is optically flat at the desired angle. Then the fiber is carefully rotated 180° and mounted on the shallower angle side of the chuck. The fiber is polished using diamond lapping films with an UltraTec fiber polisher until half of the fiber is polished. This produces a dual-taper fiber as depicted in the photograph of 73°/17° taper in Fig. 3. Typically, the fiber is polished at exactly the desired angle as set by the chuck; however, close watch must be kept on the polishing technique to avoid deviations from the set angle. The fiber must be polished against the rotation direction of the polishing stage to avoid dragging of the fiber. If the fiber is dragging, the polished angle will be smaller than the set angle from the chuck. This was observed with some fibers as explained below.

Theoretical Simulations and λ_{SPR} Calculations. The theoretical model was designed following that proposed by Ishimaru.[20] To introduce the theoretical model, we used a four-layer model (Fig. 4) based on Maxwell's equations describing the reflection of light from a layered system. The theoretical model enabled us to calculate SPR responses and estimate the SPR spectrum of a medium. Maxwell's equations are coupled first-order vector differential equations for the two field quantities, E (electric) and H (magnetic). When the tangential

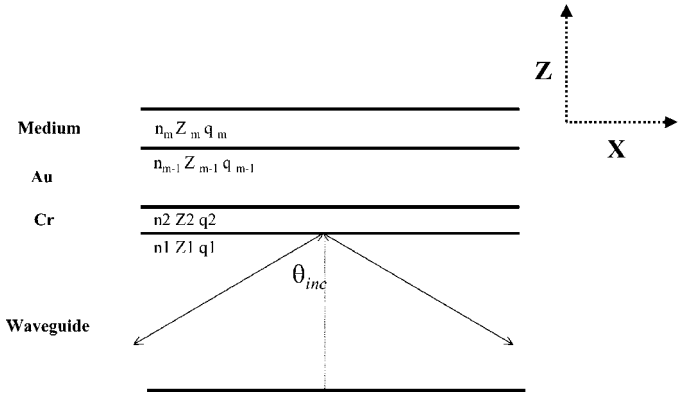

FIG. 4. The four-layer theoretical model for SPR simulations.

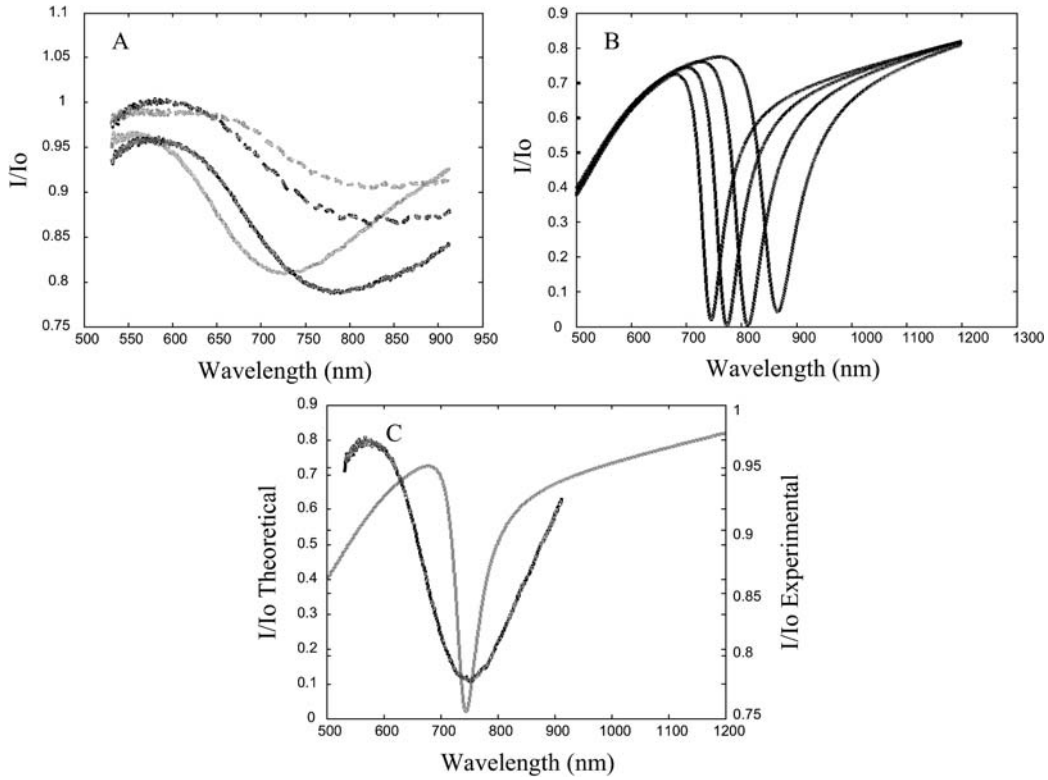

FIG. 5. (**A**) The experimental SPR spectra measurement of water 18 MΩ (RI = 1.33245 at 23.3 °C) for (gray) 73°/17°, (black) 72°/18°, (black dotted) 71°/19°, and (gray dotted) 70°/20°. (**B**) The theoretical simulations. The spectra in (B) are, from left to right, 73°/17°, 72°/18°, 71°/19°, and 70°/20°. (**C**) A comparison of the experimental and theoretical SPR spectra for a 73°/17° dual-taper SPR sensor.

electric and magnetic fields are considered as a voltage (V) and a current (I) respectively, the theoretical SPR spectrum in a layered medium can be easily generalized from the result. Ishimaru obtained the intensity reflection coefficient, R, for the total layer that can be expressed by the total $ABCD$ matrix, with the Fresnel formula

$$R = \frac{A + B/Z_t - Z_1(C + D/Z_t)}{A + B/Z_t + Z_1(C + D/Z_t)} \tag{2}$$

where $A = D = \cos ql$, $B = jZ \sin ql$, $C = (j \sin ql)/Z$, $AD - BC = 1$, and l is the thickness of the layer.

For the p polarization (TM wave),

$$V = E_x, \qquad I = H_y \qquad Z = \frac{q}{\omega\varepsilon}$$
$$q = k\cos\theta = k\left[1 - \left(\frac{n_1}{n}\right)^2 \sin^2\theta_{inc}\right]^2 \qquad k = k_0 n \tag{3}$$

where k_0 is the wave vector of the incident light, n is the refractive index, θ_{inc} is the incident angle, ω is the frequency, and ε is the dielectric constant. The MATLAB m-file for $|R|^2$ was constructed with Eqs. 2 and 3 above to obtain theoretical SPR spectra.

To estimate the minimum in the reflected light (λ_{SPR}), a second-order polynomial equation was fit to the data. The zero from the derivative curve of the second-order polynomial corresponds to λ_{SPR}. When estimating λ_{SPR} for the experimental data for straight sensors, the spectral region corresponding to the dip between 550 nm and 662 nm is used, while for the experimental data for NIR dual tapered sensors, the region between 643 nm and 913 nm is used. The theoretical data was fit between $\lambda_{SPR} - 50$ nm and $\lambda_{SPR} + 50$ nm.

Comparison Between Experimental and Theoretical Surface Plasmon Resonance Spectra for Dual-Taper Sensors. Theoretical simulations were performed to calculate the angle at which the SP band will be excited for a silica optical fiber. The thickness of the Cr layer was 2 nm while the gold layer thickness was 50 nm. The reflection spectra were calculated for aqueous solutions with a refractive index of 1.333. The theoretical SPR spectra for sensors tapered at 73°/17°, 72°/18°, 71°/19°, and 70°/20° are presented in Fig. 5B. The spectra at 73°/17° are located closer to the red region of the spectrum at $\lambda_{SPR} = 768$ nm. Decreasing the taper angle shifts the spectra toward the infrared region. The spectra represented at the longer wavelength end of the spectrum is for an SPR sensor at 70°/20° with $\lambda_{SPR} = 897$ nm. The spectrophotometer used in this study covers the range between 531 nm and 913 nm; therefore, tapering the sensor at an angle lower than 70° would yield an SPR spectrum outside the working range of the system.

The experimental SPR spectra obtained for the sensors tapered at 73°/17° (gray), 72°/18° (black), 71°/19° (black dotted), and 70°/20° (gray dotted) are presented in Fig. 5A. The experimental spectra are generally in very good agreement with the theoretical spectra, as shown in Fig. 5C for a tapered sensor at 73°/17°. The predicted λ_{SPR} for the experimental spectrum is within 40 nm of the predicted ones for every sensor prepared, with better accuracy for the sensors at 73°/17° and 72°/18°, which are within 10 nm of the predicted λ_{SPR}. The experimental spectra are broader than the theoretical spectra

TABLE I. Figures of merit for SPR sensors.

Sensing area angle/mirror angle (°)	Theoretical λ_{SPR} (nm)	Experimental λ_{SPR} (nm)	$\delta\lambda/\delta n$ (10^3 nm/RIU)
70/20	897	870 ± 1	13 ± 2
71/19	838	853.4 ± 0.6	9.2 ± 0.7
71/19	838	880.8 ± 0.8	24 ± 3
72/18	793	801.3 ± 0.1	4.6 ± 0.7
72/18	793	828.6 ± 0.4	7 ± 1
73/19	768	766.7 ± 0.1	3.3 ± 0.3
73/19	768	756.7 ± 0.2	3.2 ± 0.4
Straight	648	600.52 ± 0.07	1.9 ± 0.3
Straight	648	602.90 ± 0.04	1.6 ± 0.3

for several reasons. Most of the light is collimated using a 0.12 NA fiber. However, the non-collimated light can excite the SP at a slightly different angle, causing broadening of the spectra. To solve this problem, lower NA fibers would have to be used, which is currently limited by their commercial availability. Another source of broadening of the SPR spectra occurs during the polishing of the sensing area and the mirror. If the fiber is dragging on the diamond lapping film, the sensing area can be either at a smaller angle or slightly curved, allowing a distribution of angles on the sensing area. Moreover, if the angle between the mirror and the sensing area is not exactly 90°, the light rays hitting the sensing area first will have a different angle than the rays hitting the mirror first and then hitting the sensing area. This effect will also cause a distribution of angles at the sensing area, broadening the SPR spectra. Lastly, the quality of the gold film also affects the narrowness of the SPR spectra. A rough gold film or uneven film translates in different thicknesses of the gold film in different regions of the sensing area. This roughness will cause a broadening of the SPR spectra. Therefore, to furthermore improve the narrowness of the SPR dip, smoother gold films must be deposited on the sensor. Most sources of broadening of the SPR dip are controllable; therefore, in larger scale production of the sensors, these problems arising from handcrafting the sensors would disappear.

The position of the minimum for the SPR sensor is close to that predicted theoretically. This indicates that the sensors are polished at the desired angle. The deviations from the theoretical values of λ_{SPR} are generally red-shifted, meaning that λ_{SPR} from the experimental data is at a longer wavelength than the simulations predict (Table I). It indicates that the polishing method involves some dragging of the fiber, producing a slightly shallower angle than was set to be polished. If a 71°/19° sensor is polished, the 71° side will actually be slightly less than 71°. The theoretical λ_{SPR} for 71° is 838 nm, but both sensors yielded larger λ_{SPR} at 853.4 nm and 880.8 nm, respectively. The polished angle is therefore likely between 70° and 71°. The only exceptions are the sensors at 70° and at 73° (Table I). The sensors at 73° are very close to the theoretical value; a lower λ_{SPR} might mean that a gold layer slightly thinner than 50 nm was deposited. The gold deposition is controlled by a quartz crystal microbalance thickness monitor; however, depending on the length of the sensors the thickness can vary slightly. Longer sensors will have a thicker layer since they will be located closer to the sputtering target. Sensors are all made at 45 mm, but small differences can arise during the polishing steps. Aside from these small differences, the sensors produced are in very good agreement with theoretical simulations.

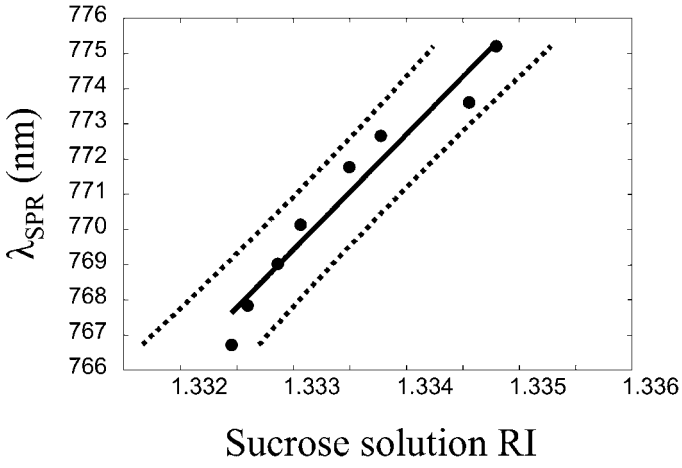

FIG. 6. Calibration curve for sucrose solutions using a dual-tapered SPR sensor. The taper is 73°/17°. The solid line represents the regression line from the least-squares linear regression and the dotted lines represent two standard deviations from the regression.

Sensitivity and Calibration of the Sucrose Solutions. Surface plasmon resonance sensors in the NIR region theoretically have greater sensitivity than those in the visible range, as was previously observed with SPR using the Kretschmann configuration.[8–10] To investigate the enhancement in sensitivity obtained by performing SPR in the NIR region, sucrose solutions ranging in mole fraction from 0 (pure water 18 MΩ) to 15×10^{-3} mole fraction sucrose in water were used. The refractive index of these solutions was accurately measured using an Abbe refractometer (DR5000, Kruss, Germany) to an accuracy of 1×10^{-5} RIU. The temperature was controlled to 23.3 ± 0.1 °C using a temperature-controlled recirculating bath. The refractive index of these sucrose solutions covers the range between 1.33245 for 0 mole fraction sucrose to 1.33479 RIU for 15×10^{-3} mole fraction sucrose in water. The solutions were measured with every SPR sensor. The temperature of the solutions was controlled using a room-temperature water bath. The sensor was immerged in the solution for 5 minutes to allow thermal equilibration. Calibration curves were obtained for the change in λ_{SPR} for sucrose solutions with different refractive indices. Figure 6 depicts a calibration curve for a dual-tapered sensor at 73°/17°. A linear regression can be applied over such a small range of refractive indices. The effect on the calibration curve of any nonlinearity in the data is negligible. Figure 6 shows that a linear model for the calibration is applicable.

The slope of the least-squares model defines the sensitivity in this study. The values for the sensitivity of different sensors are given in Table I. The straight sensors are the sensors that the authors have previously used in the detection of biomolecules.[1–3] The sensitivity of these straight sensors is between 1.6 and 1.9×10^3 nm/RIU. For the NIR sensors, the sensitivity increases exponentially (Table I). The highest observed sensitivity was observed for a 71° sensor at $(24 \pm 3) \times 10^3$ nm/RIU. This is thirteen times greater than that obtained when using straight sensors. Using a different spectrophotometer and sensors with smaller angle for the sensing area, this enhancement of the sensitivity would be even greater. Currently, in this article the spectrometer available limits the use of sensors with a taper of >70°.

Theoretical simulations also yield the predicted sensitivity for the sensors with different taper angles, as shown in Fig. 7A. The

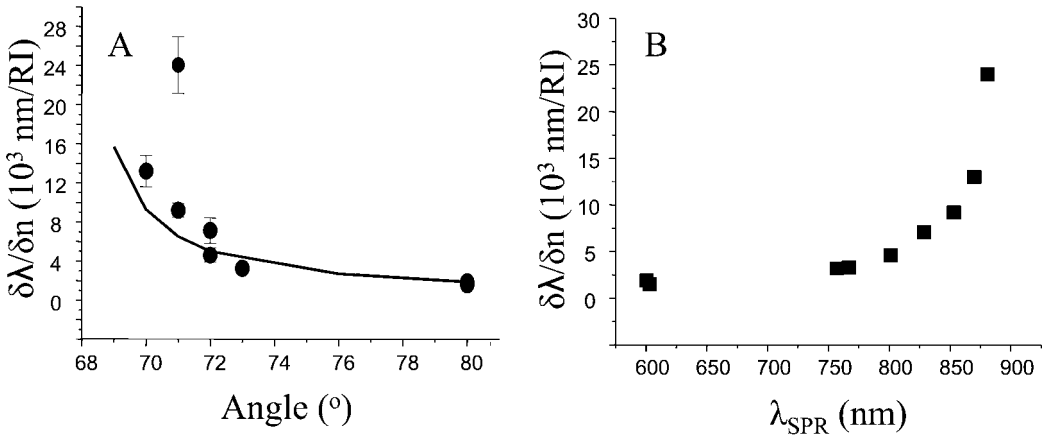

FIG. 7. The dependence of the sensitivity on the angle of incidence of the light and the wavelength. (**A**) The dependence of the sensitivity on the angle of incidence: the solid line represents the theoretical sensitivity and the circles represent the experimental data. (**B**) The experimental data for the sensitivity as a function of λ_{SPR}.

solid line in Fig. 7A represents the predicted sensitivity of the SPR sensor for an aqueous solution of 1.333 RIU. The solid circles are the experimental data for sensors manufactured at different angles. The experimental data correlates well with the prediction from the simulations, with the exception of one sensor at 71°. The exponential correlation between the angle and the sensitivity also indicates the advantage of manufacturing sensors in the NIR region. Manufacturing sensors with a taper angle smaller than 70° would yield a more sensitive sensor.

The deviations from the simulations and the experimental data are mainly from the small differences in the angle of the sensor and the thickness of the gold layer from different sensors. Figure 7B depicts the experimental sensitivity correlation with λ_{SPR} for water 18 MΩ, 1.33245 RIU. The experimental data follows a smooth, rapidly rising trend, indicating that the differences with the simulations in Fig. 7A come from the small inaccuracies in the sensor manufacturing.

Figures of Merit of the Near-Infrared Surface Plasmon Resonance Sensors. Near-infrared SPR sensors based on fiber optics with a diameter of 486 μm yields a sensing area of approximately 0.09 mm^2. The sensing area for the NIR SPR sensor presented here is smaller than most SPR imaging systems. The sensing area for typical imaging systems is approximately 0.25 mm^2, as previously reported.[21] With a combination of the sensitivity enhancement and the smaller sensing area, a huge reduction in the number of molecules detected is expected with NIR SPR. Typical detection limits with straight sensor fiber-optic SPR of approximately 10 pg/mm^2 are achieved for biomolecules. The sensing area of straight sensor fiber-optic SPR is usually 6 mm^2, resulting in an absolute detection of 60 pg. Using the smaller and more sensitive NIR SPR sensors, the detection limit for biomolecules would be approximately 1 pg/mm^2. Therefore, a sensor made of 486 μm diameter optical fiber, and a sensing area of 0.09 mm^2, would yield an absolute detection of less than 100 fg. These sensors theoretically could be manufactured with fibers as small as 100 μm in diameter, yielding detection of only a few fg.

CONCLUSION

The manufacture of fiber-optic SPR sensors working in the NIR spectral region has been achieved. These sensors are in good agreement with the theoretical simulations performed. To achieve excitation in the NIR spectral region, the geometry of the sensor was modified by polishing two tapers at the distal end of the sensor. Sensors with dual tapers of 73°/17°, 72°/18°, 71°/19°, and 70°/20° were manufactured. The largest sensitivity is observed for sensors at 71°/19° and 70°/20°. The sensitivity of SPR sensors in the NIR region is up to 13 times larger than straight sensor fiber-optic SPR sensors. Theoretical simulations show that even higher enhancement is to be expected by manufacturing dual-taper sensors with an angle smaller than 70°. The spectrometer available for this study limits the sensor angle to >70°. With these SPR-NIR sensors, sensing areas 50 times smaller than the conventional straight sensor fiber-optic SPR are easily manufactured and combined with up to thirteen-times improvement of the sensitivity; it would be possible to detect less than 100 fg adsorption of a biomolecule onto the surface.

1. T. M. Battaglia, J. F. Masson, M. R. Sierks, S. Beaudoin, J. Rogers, K. N. Foster, G. A. Holloway, and K. S. Booksh, Anal. Chem. **77,** 7016 (2005).
2. J. F. Masson, L. A. Obando, S. Beaudoin, and K. S. Booksh, Talanta **62,** 865 (2004).
3. J.-F. Masson, M. Barnhart, T. M. Battaglia, G. E. Morris, R. Nieman, P. J. Young, C. L. Lorson, and K. S. Booksh, Analyst (Cambridge, U.K.) **129,** 855 (2004).
4. G. Ramsay, *Commercial Biosensors: Applications to Clinical, Bioprocess, and Environmental Samples* (John Wiley and Sons, New York, 1998).
5. H. Raether, *Surface Plasmons on Smooth and Rough Surfaces and on Grating* (Springer-Verlag, New York, 1988).
6. R. C. Jorgenson and S. S. Yee, Sens. Actuators, B **12,** 213 (1993).
7. R. C. Jorgenson and S. S. Yee, Sens. Actuators, A **43,** 44 (1994).
8. C. Jung, S. Yee, and K. Kuhn, J. Lightwave Technol. **12,** 1802 (1994).
9. G. Brink, H. Sigl, and E. Sackmann, Sens. Actuators, B **25,** 756 (1995).
10. G. Brink, L. Schmitt, R. Tampe, and E. Sackmann, Biochim. Biophys. Acta **1196,** 227 (1994).
11. A. Ikehata, T. Roh, and Y. Ozaki, Anal. Chem. **76,** 6461 (2004).
12. A. Baba, J. Lubben, K. Tamada, and W. Knoll, Langmuir **19,** 9058 (2003).
13. H. Sigl, G. Brink, M. Seufert, M. Schulz, G. Wegner, and E. Sackmann, Eur. Biophys. J. Biophys. Lett. **25,** 249 (1997).
14. M. Zangeneh, N. Doan, E. Sambriski, and R. H. Terrill, Appl. Spectrosc. **58,** 10 (2004).
15. T. R. Jensen, M. D. Malinsky, C. L. Haynes, and R. P. Van Duyne, J. Phys. Chem. B **104,** 10549 (2000).
16. B. P. Nelson, A. G. Frutos, J. M. Brockman, and R. M. Corn, Anal. Chem. **71,** 3928 (1999).
17. A. G. Frutos, S. C. Weibel, and R. M. Corn, Anal. Chem. **71,** 3935 (1999).
18. L. A. Obando and K. S. Booksh, Anal. Chem. **71,** 5116 (1999).
19. Y. C. Kim, S. Banerji, J. F. Masson, W. Peng, and K. S. Booksh, Analyst (Cambridge, U.K.) **130,** 838 (2005).
20. A. Ishimaru, *Electromagnetic Waves Propagation, Radiation and Scattering* (Prentice Hall, New Jersey, 1991).
21. H. J. Lee, A. W. Wark, T. T. Goodrich, S. P. Fang, and R. M. Corn, Langmuir **21,** 4050 (2005).